The Effect of the Mast on Sail Performance

P. Izaguirre-Alza[1], L. Pérez Rojas[1], R. Zamora-Rodríguez[1]

([1]) Model Basin Research Group (CEHINAV), Naval Architecture School (ETSIN), Technical University of Madrid (UPM).

Abstract

In this study, the airflow around a yacht sail with imposed final geometry is simulated using a CFD (Computational Fluid Dynamics) code reproducing full scale measurements. The code is a commercial viscous CFD based on Reynolds-Averaged Navier-Stokes (RANS) equations. The purpose of this article is to consider the effect of the mast on the performance of a sail.

This research is related to a previously and published investigation written by the first author. That research was based on the aerodynamics of sails alone due to the lack of knowledge in regards to the geometry of the mast. The contribution of this new research is the calculation of how the mast affects sail performance using a recently acquired software. Furthermore, a methodology for the study of sails has been developed using this last software.

The pressure coefficient on the sail, driving and side forces are computed among other variables.. The results are compared with both reference data obtained by full scale measurements. It is concluded that there is good agreement between the current results and the reference data.

Key words

Sail, aerodynamics, CFD, mast, RANS, full scale.

1.- Introduction

The motivation to carry out this research began with a preceding work about the numerical study of sail performance (Izaguirre et al. 2008) by means of full scale data obtained from (Masuyama et al. 1997) and (Masuyama et al. 2007). In those papers it is described how Masuyama and Fukasawa were encouraged by Milgram's work (Milgram 1993) and built the sail dynamometer boat *Fujin*. They presented the aerodynamic coefficients for the upwind condition of International Measurement System (IMS) type sails.

In the author's aforementioned previous work, three configurations were simulated with the ANSYS-CFX (ANSYS 2008) solver, but without the geometry of the mast. The results were satisfactory but there was an interest to know how could the mast affect the sail performance. Once the geometry of the mast was available, it was considered to continue the previous research by adding the mast to the simulations.

Masts are a fundamental part of any sailing vessel because if they are not well designed, they can reduce drastically the efficiency of sails. Masts disrupt the flow at the leading edge of mainsails and usually, they create separation of the flow. From a modeling point of view, the flows become a lot more complex to model when masts are included. As demonstrated in Paton & Morvan (2007), an effective mast design can surprisingly improve sail performance.

The specific problem that it is discussed in this paper, it's a previously studied configuration in which the mast has been added. Unlike the preceding work, the simulations have been performed with the CD-Adapco's STAR-CCM+ (CD-Adapco 2009). It is expected to evaluate the effect of the mast on a mainsail without any jib.

In this paper there are presented calculated variables such as the pressure distribution over the sail, driving and side force coefficients which are compared with the reference data measured at full scale (Masuyama et al. 2009).

Furthermore, the vortices generation and the development of vorticity downstream have been thoroughly observed, which were not considered in the previous research. These phenomena are more and more relevant as it is stressed in Spenkuch et al. (2008). It is important to understand correctly these phenomena because they are critical to identify the blanketing effect between two yacht. At present time, the quantification of the “blanketing” effect is on the increase.

The remainder of this paper is organized into five sections. The geometry and the

reference data are described in the second section. Then, the numerical modeling is described. In section 4, the results are presented. Finally, conclusions are drawn in the last section.

2.- Geometry and reference data

As it has been mentioned before, in the references papers, it is described the sail performance of different configurations which were measured using the sail dynamometer boat Fujin. This boat is based upon the YR-10,3m class, in which load cells and cameras were installed to measure the sail forces and shapes simultaneously. The sailing conditions of the boat, such as boat speed, heel angle, wind speed and wind angle were recorded. This boat has an overall length of 10,35 m, a maximum beam of 3,37m and a displacement of 3,86t.

The configuration that is presented in this paper, named ID 9807172F, as in the reference papers, includes the mainsail of the Fujin. Table 1 shows the sailing condition of this configuration and the measured data at full scale such as the driving (thrust) and side force coefficients (C_X and C_Y), as well as the longitudinal and vertical position of the center of effort (X_{CE} and Z_{CE}).

The recorded data in the Fujin contained some variation due to wind fluctuation, wave reflection on the hull and the steering compensation. In Masuyama et al. (2009) the variation of each variable for all the configuration was estimated. For the configuration in study in the present research, the variations are approximately ±95% for C_X, ±20% for C_Y, ±10% for Z_{CE} and 11% for X_{CE}. The reason for the wide errors in this configuration, according to the reference paper, is that when there is no jib, it is difficult to steer adequately and the deviation in apparent wind angle becomes larger.

Configuration	9807172F
Heel angle	8,8º
Apparent wind angle	30,5º
Apparent wind speed (V)	7,3 m/s
C_X	0,290
C_Y	1,240
X_{CE}	1,560 m
Z_{CE}	5,670 m

Table 1. Sailing condition and measured data (Masuyama et al. 2009)

The origin of the coordinate system is located at the aft face of the mast at the deck level. The local reference system is: x-direction from bow to stern, y-direction from port to starboard and z-direction perpendicular to the previous directions and positive upward. In global reference system (for the CFD) the x-direction is the flow direction, the z-direction is upward and y-direction is perpendicular to the previous and right-handed.

The shape of the mainsail is provided by six points in each of the six sections in which the sail has been divided (Masuyama et al. 1997). This set of points has been introduced into Rhinoceros® 4.0, where the sail surface has been modeled.

The principal dimensions of the mainsail are:

- Peak height: 13,82 m
- Luff length:12,50 m
- Foot length: 4,44 m
- Mainsail area (S): 33,20 m^2

As aforementioned, in the previous study (Izaguirre et al. 2008) the geometry of the mast was unknown and due to this fact, the research was mainly carried out with the sails alone. Recently, Prof. Yutaka Masuyama, co-author of the references papers, sent us the section of the mast. This section has a flat back and is often described as bullet shaped section. This section has been modeled to obtain the three-dimensional geometry of the mast by assuming that the section is constant along its length.

In this article, three cases of the 9807172F configuration are presented: the “sail case” which is the sail alone, the “mast case” which only includes the mast and finally, the “rig case” which encompasses both the mast and the sail.

3.- Numerical modeling

The numerical simulations have been performed using the computational fluid dynamic software CD-Adapco's STAR-CCM+ 4.06.011, which is a Reynolds Averaged Navier Stokes Equations based solver. This software delivers the entire engineering simulation process in a single integrated environment. It is a user friendly

software that includes the latest physical models and solver technology such as innovative meshing, model set-up iterative design studies, turbulence models, transition models, cavitation, six degree of freedom motion, among others.

The calculations of this study have been run on two computers. The first computer is an Intel Core 2 Quad CPU with a Linux 2.6.31-20-generic. This computer has been used for the first studies with small meshes. Then, for larger meshes, a 8 Quad-Core cluster with a Linux 2.6.27-19-5 kernel (amd64), has been used. As an example, for a $3{,}5 \cdot 10^6$ elements mesh, the typical CPU time to achieve the desired convergence has been around 8 hours using 7 processors of the cluster. As explained in (Izaguirre et al. 2008), a similar simulation with the ANSYS-CFX took around 11 hours with a mesh of $1{,}3 \cdot 10^6$ elements.

The increase of computational time with the increasing number of mesh elements has been analysed. As it can be seen in Figure 1, the relationship between the increase of number of elements and the elapsed time per iteration is linear. The values of the abscissa as been normalized with the shortest mesh which had 72493 elements. This linear tendency is also fulfilled for the second computer. This previous analysis helps optimizing the computational time and planning the research more adequately.

Domain

The computational domain is a rectangular box. The extends of the box are set so as to permit a good development of the flow without creating wall effects. It is important to minimize the volume in order not to waste computational efforts The extension of the computational control volume has been finally set to: 10m upstream, 30m downstream, 15m to leeward, 10m windward, 0,2m below and 20m above. This overall domain is smaller than the one used in the previous study with the ANSYS-CFX but it has been checked to be sufficient.

Mesh

The meshing procedure has been conducted in the STAR-CCM+ with its own meshing tool. The final mesh is surface remesher and trimmer with prism layer mesher to properly capture the phenomena involved near the sail.

The variable Wall Y^+ has been studied to evaluate the quality of the mesh next to the rig and its capability of detecting the boundary layer by the numerical wall treatments. A typical target value of $Y^+=1$ has been aimed for most of the sail and mast surfaces, which is in accordance with the values used by (Paton & Morvan 2009) or (Spenkuch et al. 2008). Only a few cells have values over this target but they have been proved to be negligible.

For the three cases in study, the convergence of the results with the increasing number of elements have also been checked, as it can be seen in Figure 2. The simulation meshes for which results are presented in this paper consisted of anywhere between 2,5 - 13 million elements.

Solution method

The physical models utilized in these simulations are: Three-dimensional, Stationary, Turbulent, SST K-Omega, Segregated flow model, Constant density, Implicit unsteady and All y^+ Wall Treatment. In the computations, the Reynolds number has been 6,5·10 (based on the apparent wind speed and mast height).

The Segregated Flow Model is suitable for constant density flows as it is supposed they are in these simulations. This model solves the flow equations (one for each component of velocity, and one for pressure) in a segregated sequence. The linkage between the momentum and continuity equations is achieved with a predictor-corrector approach. Due to the fact that the time scales of the phenomena of interest are of the same order as the convection and diffusion processes, the implicit unsteady approach is recommended. In the implicit unsteady approach each physical time-step involves some number of inner iterations to converge the solution for that given instant of time. The time step has been set to 0.1s for all the simulations and the inner iterations to 5. The time step is around the 15% of the characteristic time which is the characteristic length (~5m) divided by the speed (7,3 m/s).

As usual, in order to close the RANS equations and determine the Reynolds stresses a turbulence model is required. The model chosen has been the SST (Shear Stress Transport) as in (Hutchins 2008), (Ciortan & Guedes-Soares 2007), (Clauss & Heisen 2005) or (Quérard & Wilson 2007).

This model was developed in 1994 by Menter. The SST accounts for the transport of the turbulent shear stress and gives highly accurate predictions of the onset and the amount of flow separation under adverse pressure gradients. The SST is one of the most popular turbulence models in external aerodynamics and it is used widely in the industry. The reason for the wide spread usage of this model in aeronautics is that it is robust; it allows an integration through the viscous sublayer without much computational effort and has advanced separation prediction capabilities, (Menter & Egorov 2007).

It is important to choose an appropriate wall treatment among this software's supplies, in order to capture the phenomena involved near the rig and resolve the viscous-affected region. In this case, the All Wall y^+ Treatment has been set. This options is the most general treatment that encompassed both the high-y^+ and the low-y^+. Furthermore, this treatment distinguish automatically between them.

In order to judge convergence the value of the RMS (root mean square) residual has been considered. A maximum RMS of 10^{-4} has been obtained for all runs but in most simulations, noticeably lower residuals have been achieved. The driving and side forces have been also monitored to ensure they had settled.

Boundary conditions

The following boundary conditions have been set up:

- Velocity inlet at the inflow with the apparent wind speed intensity. The wind gradient has not been considered for numerical calculations as it was proved in Masuyama et al. (2007) that the effect was insignificant. This means that the apparent wind angle and speed are assumed to be constant along the vertical direction.
- Pressure outlet at the outflow. The averaged pressure over this surface has been set to zero.
- Walls, the ceiling and the floor has been considered slip walls. It has been checked that if the floor is set as no-slip wall the effect to the sail performance is negligible.
- Both the mast and the mainsail have been established as no-slip walls.

4.- Results

One of the benefits of these commercial codes is that they give a great amount of outputs. In this study, it has paid attention to the values which were useful to understand the phenomena involved and to compare with the data of the reference papers.

Aerodynamic force coefficients

As it can be seen in Table 2, the driving and side force coefficients have been calculated for the three cases in study. In the same table the reference data have been included again, in order to facilitate the comparison.

	Ref.	SAIL	SAIL+MAST	RIG
C_X	0,290	0,310	0,296	0,277
C_Y	1,240	1,274	1,285	1,096

Table 2. Driving force and side force coefficients.

The inclusion of the mast decreases C_X both in the “rig case” and in the sum of the “sail case” plus “mast case”, which is presented in the fourth column of the table. The inclusion of the mast improves the results that differ less than a 5%. Nevertheless, although in the “sail+mast” case the value of C_Y gets better, the “rig case” doesn't in comparison with the “sail case”.

As shown in Table 3, the longitudinal position of the center of effort has been calculated (X_{CE}), as well as the vertical position (Z_{CE}), for the “sail” and “rig” cases.

	Ref.	SAIL	RIG
X_{CE} (m)	1,560	1,951	1,791
Z_{CE} (m)	5,670	6,320	6,309

Table 3. Position of the center of effort

X_{CE} is moved forward by about 9% by the inclusion of the mast in the “rig case”, and the resultant value is closer to the full scale measurements. On the other hand, the difference in Z_{CE} between the “sail case” and the “rig case” are insignificant and both values overpredict the reference value only around a 10%.

It can be concluded that in general, taking into account the mast is more realistic and will result in improved prediction of the flow and the aerodynamic forces as far as the current configuration and sailing conditions are concerned.

Distribution of the pressure coefficient

The pressure coefficient distribution over the sail has been plotted for the “sail” and “rig”

cases. In Figure 3, the distribution over the sail in the “sail case” is presented both for the windward side and the leeward side. Similarly, Figure 4 shows the pressure coefficient distribution in the “rig case”.

The images have been compared with the numerical results by Masuyama et al. (2009) and they are similar. The pictures of pressure coefficient of the reference paper are not included in this document because of their poor resolution.

The results of the “sail case” are subtly closer to the numerical results of the reference paper because in that case the mast wasn't simulated either. Comparing both current cases, it can be concluded that the general features of the pressure distribution on the mainsail alone are similar to those for the “rig case”.

Flow detachment and upwash

The local flow field on the horizontal midsection of the mainsail is shown in Figure 5 as well as the normalized velocity distribution for both the “sail case” and the “rig case”. Upwash is a remarkable feature of the flow that is presented in both cases. Upwash is the changing of the direction of the flow as it approaches the sail (Paton & Morvan 2007). It is important to consider this phenomenon when designing an optimum sail performance.

In this pictures it can also be seen that there is a detachment of the flow in both cases even though it is more notorious in the “rig case”, where there is a vortex at the trailing edge. Even if it is usually considered that when upwind there is no separation and potential methods are used, it is demonstrated that there is separation of the flow. Because of this fact, viscous CFD codes should be use as the one in this work.

Pressure coefficient

The calculated pressure distributions on the midsection of the mainsail for two cases are presented in Figure 6. In this plot the usual aerodynamic convention of reversing the vertical scales have been used: the leeward surface pressures that are negative on the top part of the curve and the windward surface pressures that are usually positive, on the bottom part of the curve. As usually, the difference between the leeward surface and windward surface curves at a given point on the sail represent the pressure difference across the sail.

On the windward surface the flow appears to have similar trends although there are variations in values at the leading edge. On the other hand, the pressures distribution on the “sail case” are much higher (more negative) when the mast is not considered. The sail develops more lift when it is operating in a flow field created without the mast. For both cases, the trailing edge of the mainsail is in high speed region of flow created on the leeward side of the mainsail.

In summary, the influence of the mast is focused on the leeward side of the mainsail where there is a turbulent detachment of the flow. The mast reduces the efficiency of the mainsail.

Generation of vortices

As mentioned before, it is important to study the generation of vortices in order to understand the blanketing effect caused by the upwind yacht's sails and its effect on the flow propagating downwind which reduces its magnitude and alters its direction.

Figure 7 shows the streamlines in the flow field to identify the influence of the mast by comparison of the two cases. As it can be seen in the present results, the influence of the mast on flow is particularly significant. Two main vortices are generated at the “rig case”: one at the top of the mast and the other at the end of the foot of the mainsail. On the other hand, the “sail case” seems to have smooth streamlines. The reason of this difference between the cases can be the density of the mesh. Even thought near the sail the meshes are similar, in the far field, the mesh of the “sail case” is coarser than the “rig case”. Maybe, the mesh of the case without the mast cannot detect the vortices as well as it happens in the next section.

G) VORTICITY

Figure 8 displays the development of the maximal vorticity downstream of the mainsail. This phenomenon is also important when studying the blanketing effect.

It can be observed that the vorticity values have different starting values and decrease exponential. The steep decrease in vortex strength continues up to the value of 2-3 foot lengths downstream and decelerates afterwards. It is noteworthy the increase of the vorticity values due to the inclusion of

the mast although maybe it is not only because of the mast. In this section, the quality of the mesh downstream can also vary the results and a fine resolution is needed. Therefore, it would be necessary to improve the quality of the mast in the “sail case” and study this improvement on both the generation of vortices and the development of vorticity.

5.- Conclusions

Through the analysis of the results, it appears that the trends of the flow and the measured variables of the reference data are fairly well predicted by the present simulations.

Acknowledgements

The research that this paper contains has been funded by an UPM PhD scholarship. Also, a special thanks to Prof. Yutaka Masuyama for his helpful information.

References

ANSYS 2008, *ANSYS CFX-Solver, Release 10.0: Modelling*.

Brandt, H, Hochkirch, K. (2000). *Entwicklung einer meßyacht zur analyse der segelleistung im orginalmaßstab (Design and Construction of a full scale Measurement System for the Analysis of Sailing Performance)*, Tech. rep., Technische Universität Berlin (Germany).

Caponnetto, M., Castelli, A., Dupont, P., Bonjour, B., Mathey, P.L., Sanchi, S., Sawley, M.L. (1999). *Sailing Yacht Design Using Advanced Numerical Flow Techniques*, in: 14th Chesapeake Sailing Yacht Symposium, Annapolis, Maryland (USA).

CD-Adapco (2009). User guide, STAR-CCM+ Version 4.06.011.

Ciortan, C. Guedes-Soares, C. (2007). *Computational Study of Sail Performance in Upwind Condition*, Ocean Engineering, number 34, pages 2198-2206.

Clauss, G., Heisen, W. (2005). *CFD Analysis on the Flying Shape of Modern Yacht Sails*, in: 12th International Congress of the International Maritime Association of the Mediterranean, Lisbon (Portugal).

Collie, S.J., Jackson, P.S., Gerritsen, M. (2002) *Validation of CFD Methods for Downwind Sail Design*, in: 1st High Performance Yacht Design Conference, Auckland (New Zealand).

Collie, S.J., Jackson, P.S., Gerritsen, M., Fallow, J.B. (2004) *Two Dimensional CFD Based Parametric Analysis of Downwind Sail Designs*, RINA.

Hansen, H., Jackson, P.S., Hochkirch, K. (2002). *Comparison of Wind Tunnel and Full-Scale Aerodynamic Sail Force Measurements*, in: 1st High Performance Yacht Design Conference, Auckland (New Zealand).

Hutchings, N. (2008) *The Use of ANSYS CFX in America's Cup Yacht Design,* in: 3rd High Performance Yacht Design Conference, Auckland (New Zealand).

Izaguirre, P., Zamora, R., Pérez, L. (2008). *Computational Study of Sail Performance of a Racing Yacht*, 47º Congreso de Ingeniería Naval e Industria Marítima, Palma de Mallorca (Spain).

Jones, P., Korpus, R. (2001) *International America's Cup Class Yacht Design Using Viscous Flow CFD*, in: 15th Chesapeake Sailing Yacht Symposium, Annapolis, Maryland (USA).

Lasher, W.C. (1999). *On the Application of RANS Simulation for Downwind Sail Aerodynamics*, in: 14th Chesapeake Sailing Yacht Symposium, Annapolis, Maryland (USA).

Lasher, W.C., Sonnenmeier, J.R. (2008). *An Analysis of Practical RANS Simulations for Spinnaker Aerodynamics*, Journal of Wind Engineering and Industrial Aerodynamics, number 96, pages 143-165.

Masuyama, Y., Fukasawa, T. (1997). *Full Scale Measurement of Sail Force and Validation of Numerical Calculation Method*, in: 13th Chesapeake Sailing Yacht Symposium, Annapolis, Maryland (USA).

Masuyama, Y, Tahara, Y., Fukasawa, T., Maeda, N. (2007). *Database of Sail Shapes vs. Sail Performance and Validation of Numerical Calculation for Upwind Condition,* in: 18th Chesapeake Sailing Yacht Symposium, Annapolis, Maryland (USA).

Masuyama, Y, Tahara, Y., Fukasawa, T., Maeda, N. (2009). *Database of Sail Shapes versus Sail Performance and Validation of Numerical Calculation for Upwind Condition,* Journal of Marine Science and Technology 14, 137-160.

Menter, F., Egorov, Y., (2007) *Turbulence Modeling of Aerodynamic flows*, in: International Aerospace CFD Conference, Paris (France).

Milgram, J.H. Peters, D.B., Eckhouse, N. (1993) *Modeling IACC Sail Forces by Combining Measurements with CFD*, in: 11th Chesapeake Sailing Yacht Symposium, Annapolis, Maryland (USA).

Paton, J.S., Morvan, H.P. (2007). *The Effect of Mast Rotation and Shape on the Performance of Sails*, International Journal of Maritime Engineering.

Paton, J.S., Morvan, H.P. (2009). *Using Computational Fluid Dynamics to Model Sail*

Interaction- the "Slot Effect" Revised, Journal of Wind Engineering and Industrial Aerodynamics.

Quérard, A.B.G. Wilson, P.A. (2007). *Aerodynamic of Modern Square Head Sails: a Comparative Study between Wind Tunnel Experiments and RANS Simulations*, International Journal of Small Craft Technology, number 147.

Richter, H.J., Horrigan, K.C., Braun, J.B. (2003) *Computational Fluid Dynamics for Downwind Sails*, in: 16th Chesapeake Sailing Yacht Symposium, Annapolis, Maryland (USA).

Shankaran, S., Doyle, T., Gerritsen, M., Iaccarino, G., Jameson, A. (2002) *Improving the Design of Sails using CFD and Optimization Algorithms*, in: 1st High Performance Yacht Design Conference, Auckland (New Zealand).

Spenkuch, T., Turnock, S., Scarponi, M., Shenoi, A. (2008) *Lifting Line Method for Modelling Covering and Blanketing Effects for Yacht Fleet Race Simulation*, in: 3rd High Performance Yacht Design Conference, Auckland (New Zealand).

Yoo, J., Kim, H.T. (2006) *Computational and Experimental Study on Performance of Sails of a Yacht*, Ocean Engineering, number 33, pages 1322–1342.

Appendix A: Pictures and Charts

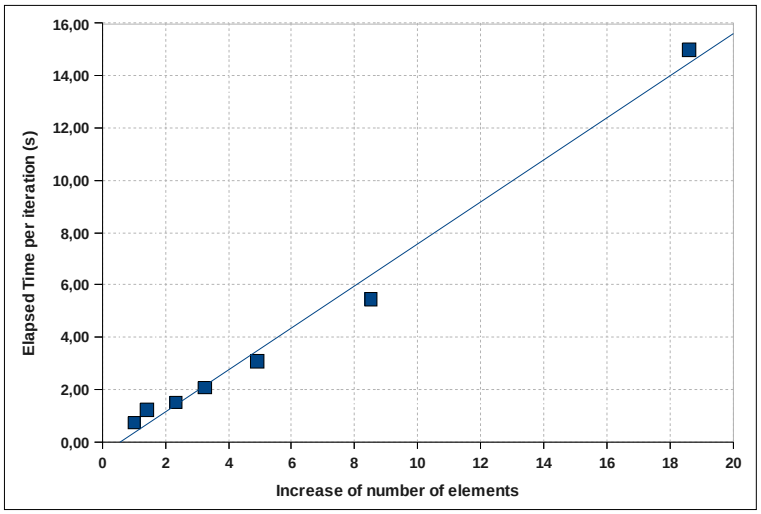

Figure 1. Increase of the number of elements vs. elapsed time per iteration. “Mast case” with computer 1.

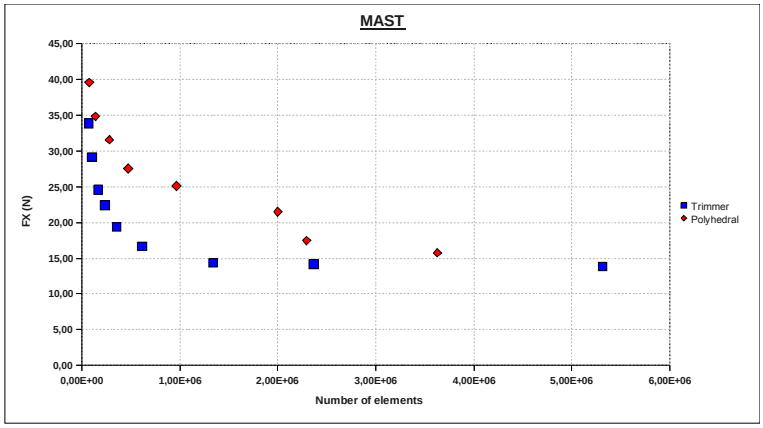

Figure 2. Convergence of the mast driving force. “Mast case”.

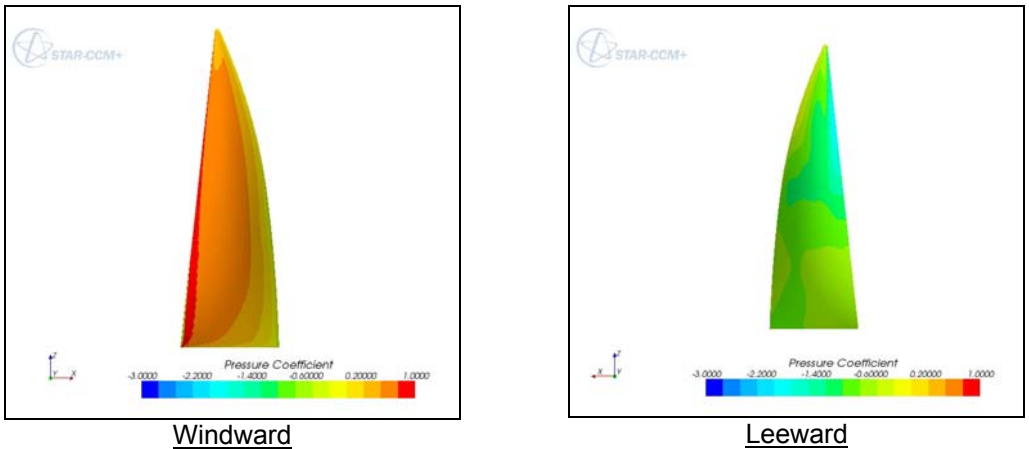

Windward Leeward

Figure 3. Distribution of pressure coefficient over the sail in the “sail case”

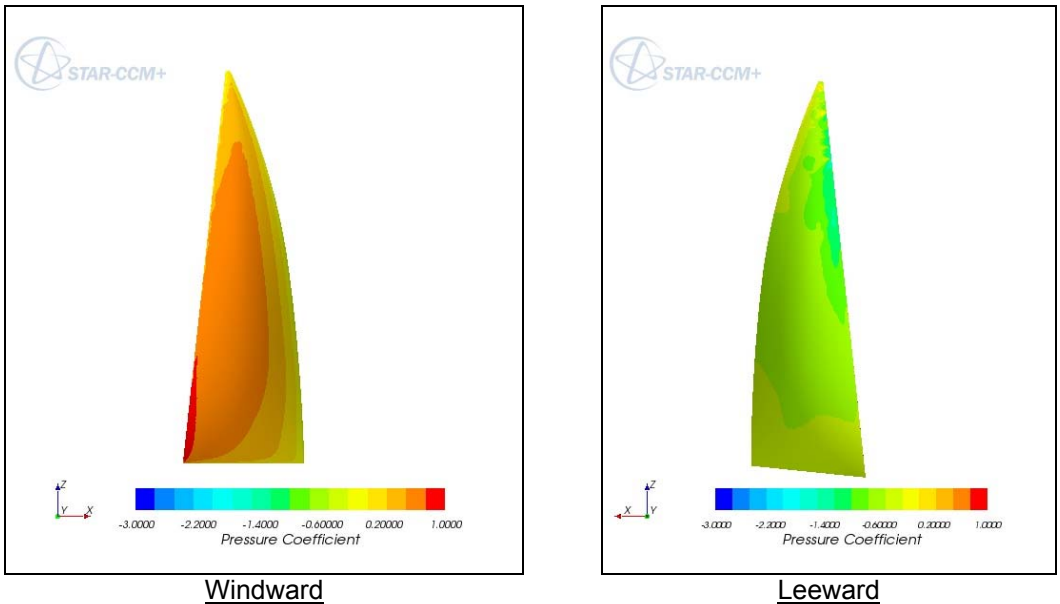

Windward Leeward

Figure 4. Distribution of pressure coefficient over the sail in the "rig case"

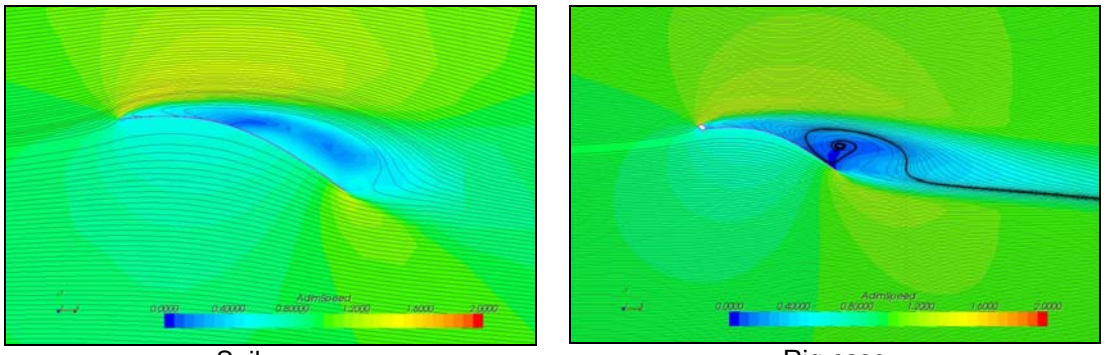

Sail case Rig case

Figure 5. Normalised speed and streamlines

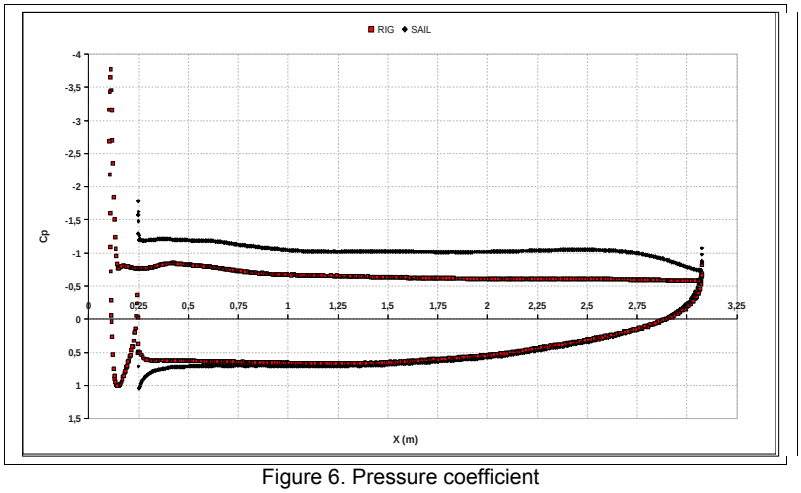

Figure 6. Pressure coefficient

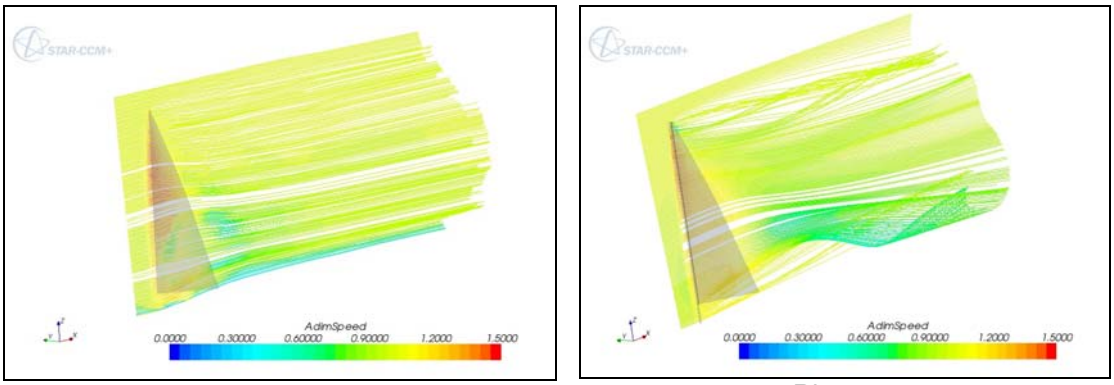

Sail case Rig case

Figure 7. Generation of vortices

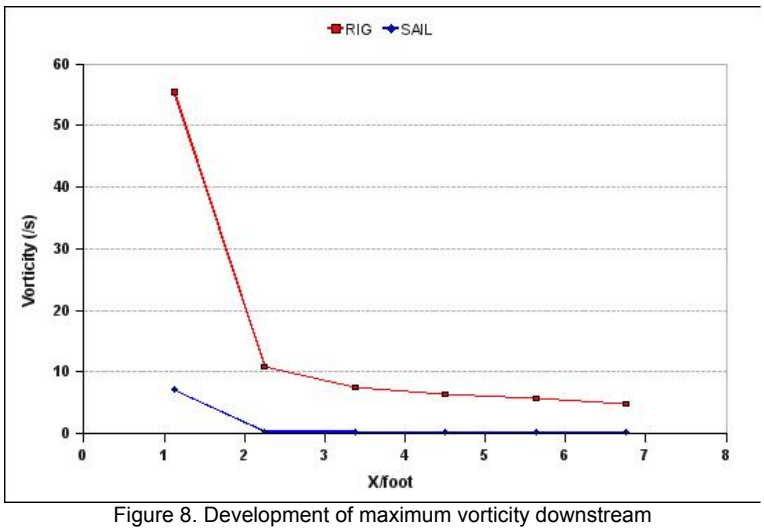

Figure 8. Development of maximum vorticity downstream